Water Resources Research

Key Points:
- For imaging aquifer heterogeneity, moving single excitation is better than periodic excitations
- As long as the signal-to-noise ratio is large, the resolution of images is independent of the amplitude and frequency of excitation
- Spatial sampling interval should be less than a quarter of the correlation length

Resolution and Ergodicity Issues of River Stage Tomography With Different Excitations

Yu-Li Wang[1], Tian-Chyi Jim Yeh[2,1], Jet-Chau Wen[3,4], Xu Gao[5], Zaiyong Zhang[6], and Shao-Yang Huang[4]

[1]Department of Hydrology and Atmospheric Sciences, University of Arizona, Tucson, AZ, United States, [2]Tianjin Key Laboratory of Water Resources and Environment, Tianjin Normal University, Tianjin, China, [3]Department of Safety, Health, and Environmental Engineering, National Yunlin University of Science and Technology, Douliu, Taiwan, [4]Research Center for Soil and Water Resources and Natural Disaster Prevention, National Yunlin University of Science and Technology, Douliu, Taiwan, [5]Faculty of Engineering, China University of Geosciences, Wuhan, China, [6]Key Laboratory of Subsurface Hydrology and Ecological Effects in Arid Region, Chang'an University, Xi'an, China

Abstract This study investigates spatiotemporal cross correlation between the observed head and the hydraulic diffusivity parameters in heterogeneous aquifers under static and migrating periodic excitations with different frequencies and other factors and a moving single excitation along a river boundary. Results of the cross-correlation analysis are verified by estimating the parameters in a synthetic heterogeneous aquifer under these excitations. For assuring the statistical significance of the results based on a single realization, Monte Carlo experiments of estimating the parameters with these excitations are conducted. The experiments also explore the relationship between the resolution of the estimated parameters and the distance from the excitation to the observation wells, the frequency, and amplitude of the excitation and the mean diffusivity of the aquifer. In addition, the relationship between the resolution of the estimates and monitoring network spatial density is investigated. Finally, the usefulness of moving single excitations, effects of frequencies of the periodic excitations under different situations, the density of monitoring network in term of correlation scale, and the ergodicity issue corresponding to the number of observation and size of simulation domain are discussed.

1. Introduction

Proper management of groundwater resources requires accurate knowledge of the water balance (i.e., storage, inflow, and outflow) and spatiotemporal distributions of water bodies with different chemistries (e.g., contaminants or salinity). These states are controlled by the subsurface hydrologic and geological structures. As a result, many techniques for characterizing subsurface characteristics have been developed in the past. One of the leading new techniques is hydraulic tomography (HT). The HT survey is built upon the human instinct: viewing an object from different angles and perspectives to obtain nonredundant information and synthesizing these pieces of information to gain a full description of the object. Following this logic, an HT survey sequentially perturbs (e.g., injecting, pumping, or slug test) an aquifer at different locations and monitors heads at many observation wells. An appropriate inverse model then assimilates all the information to portrait distributions of spatially varying aquifer properties.

Over past decades, HT has become a matured aquifer characterization technology at small-scale field sites (e.g., Berg & Illman, 2011, 2013; Bohling et al., 2002; Brauchler et al., 2003, 2007, 2011, 2013; Cardiff et al., 2012, 2013; Hochstetler et al., 2016; Huang et al., 2011; Li et al., 2008; Paradis et al., 2016; Sanchez-León et al., 2016; Straface et al., 2007; Zhao & Illman, 2017).

For basin-scale (hundreds or thousands of square kilometers) aquifer characterizations, large pumping rates are required to produce noticeable groundwater level responses over the entire basin. This makes applications for basin-scale aquifer characterization impractical. Therefore, taking advantage of municipal well fields and their production scheduling as a basin-wide aquifer characterization method becomes a potential option (Yeh & Lee, 2007). Similarly, exploiting natural events (such as lightning, earthquake, storm, typhoon, tide, or even atmospheric pressure variations) as spatial and temporal varying excitation sources for basin-scale hydraulic tomographic surveys has been proposed by Yeh et al. (2008).

Numerous studies have been conducted in the past to estimate the hydrogeologic properties of aquifers by interpreting the aquifer response due to river stage variations. Using sinusoidal wave and one-dimensional homogeneous confined aquifer assumptions, Ferris (1952); Ferris et al. (1963) presents analytical methods (i.e., time lag and stage ratio) for calculating aquifer diffusivity based on well hydrographs in response to river-stage variations. Nevulis et al. (1989) applied these methods to a field site. Gelhar (1974), Duffy et al. (1978), and Gelhar et al. (1979) utilized a spectral approach to estimate transmissivity and storage coefficient of homogeneous aquifers by using the relationship between the well hydrograph and the stream variation.

Parallel to the aforementioned studies, two-dimensional analytical solutions of groundwater variations of homogeneous confined aquifers in response to tidal loading along the shoreline were developed by Sun (1997) and for leaky confined aquifer by Jiao and Tang (1999), Li and Jiao (2001), and Tang and Jiao (2001). Similarly, Li et al. (2000) and Li et al. (2002) derived the solution describing the groundwater variations near the estuary, where the tidal loadings in river and ocean are significant, to estimate the diffusivity of homogeneous confined aquifers. On the other hand, Pinder et al. (1969), Barlow et al. (2000), and Moench and Barlow (2000) developed convolution methods to investigate the groundwater variations of homogeneous confined aquifers in response to any arbitrary impulse along a line boundary.

Following the ideas of Yeh et al. (2008) for exploiting natural stimuli as sources of basin-scale aquifer hydraulic tomographic surveys, Yeh et al. (2009) conducted numerical experiments to demonstrate the feasibility of river stage tomography for characterizing basin-scale subsurface heterogeneity using aquifer responses to the propagation of a flood wave. Wang et al. (2017) applied the river stage tomography to a real-world scenario in which seasonal river stage variations were used as the excitation sources for characterizing an alluvial fan in Taiwan.

It is important to emphasize that the aquifer characterization studies as well as the river stage tomography discussed previously make use of the groundwater pressure responses due to river stage fluctuations, rather than the actual water exchange between the river and the adjacent aquifers as presented in the studies by Vazquez-Sune et al. (2007) and Brunner et al. (2017). The rationale rests upon the fact that the pressure responses of the aquifer (e.g., from few centimeters to several tens of centimeters) to the river excitations can propagate for up to tens of kilometers in confined or semiconfined aquifer as substantiated by the field observations (e.g., Sophocleous, 1991, Promma et al., 2007, Jardani et al., 2012, Ramirez-Hernandez et al., 2013, Hsiao et al., 2017, Wang et al., 2017, and others), while actual flow exchanges between river and groundwater are often limited to hundreds of meters at most. For example, Sophocleous (1991) reported that there are at least 0.25 ft head changes (site #5) in response to the river fluctuation at a long distance (10 km away from the river) in a "conceptually" confined aquifer in Kansas, USA (Figures 10 and 11 in Sophocleous, 1991). Similarly, Jardani et al. (2012) showed that the amplitude of groundwater level of a "semiconfined" aquifer (again a conceptualized term) is 0.1 m at the well 3 km away from the Seine River at Upper Normandy, France (Figure 8 in Jardani et al., 2012). This groundwater level amplitude corresponds to a 1.1-m stream stage fluctuation. Likewise, the study of groundwater responses to controlled water releases of the Colorado River in Mexico reported a 0.6-m response in the groundwater at the well (well 9) 3 km away from the river (Figure 6 in Ramirez-Hernandez et al., 2013). Moreover, Promma et al. (2007) reported the seasonal groundwater level variations measured at Phitsanulok, Thailand, are influenced by the river 3 km away from the well (well 14; Figure 6 in Promma et al., 2007). The groundwater level rises 3 m in 3 months accompanied with a 4-m rise of the river stage (Y3 in Figure 6 in Promma et al., 2007).

Albeit the river stage tomography based on single flood event and seasonal river stage variations have been investigated previously, the river stage may vary in different forms at different frequencies due to many environmental factors and human activities. Impacts of these different variations on the efficiency of the river stage tomography using different groundwater monitoring networks for basin-scale aquifer characterization remain unknown.

Therefore, investigation of the effects of different river stage variations and the monitoring network design on the large-scale aquifer characterization are the objectives of this study. For these purposes, this study first investigates the cross correlations between the head at a well and the variation of diffusivity parameter (D) at different parts of aquifers under static periodic, migrating periodic, and moving single excitations since the cross correlations are the key to the aquifer parameter identification. These selected excitations could represent hourly, daily, monthly, and seasonal variations of the river stages (or a large water body) due to tidal
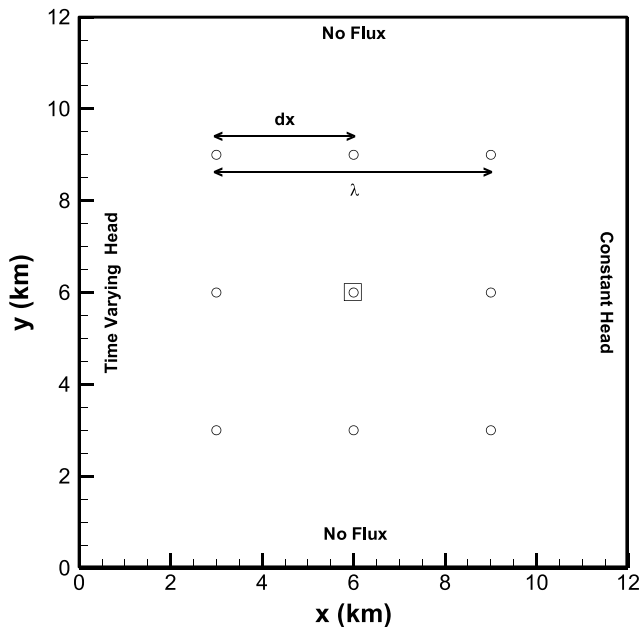
Figure 1. Two-dimensional horizontal domain utilized in this study. The upper and lower boundaries are no flux while the right boundary is the constant head. A prescribed time-varying river stage variation is assigned to the left boundary. The circles represent the monitoring wells. The squared circle represents the well utilized in the cross-correlation analysis. λ is the correlation scale of diffusivity and dx is the interval between wells.

effects, precipitations, climate changes, and other natural environment events. Afterward, estimation of the diffusivity field of a synthetic heterogeneous aquifer is conducted to test the findings from the cross-correlation analysis. Because the estimation based on a limited number of observed groundwater responses always involves uncertainty and the cross correlation is a probabilistic analysis, the test using a single reference field is likely inconclusive. Monte Carlo simulation subsequently follows to confirm the test results, including the effects of periodic excitations with different frequencies and network design on the high-resolution characterization of aquifers. Finally, the ergodicity issue corresponding to the number of observation and size of the simulation domain and some caveats of the implementation of river stage tomography in the field are discussed.

2. Simulations of Groundwater Responses

This section describes the numerical setup for simulating groundwater responses to different river-stage variations, which are to be used in the later analyses.

2.1. Simulation Domain Configuration

A two-dimensional horizontal domain of 40×40 square elements is created as the confined aquifer. Each element is $0.025\ [-] \times 0.025\ [-]$ in the dimensionless scale (or $300\ [m] \times 300\ [m]$ in the dimensional scale). The eastern boundary of this aquifer is a constant head boundary (30 m) while the northern and southern boundaries are no-flow boundaries. A prescribed time-varying head boundary is assigned to the west side of the aquifer (Figure 1), which represents a river fully penetrating the confined aquifer. These boundary conditions are selected to represent the propagation of the river stage fluctuation away from the river over a portion of a large river/aquifer system. The initial head is uniform (30 m) everywhere. At least 32 time steps are utilized for a single periodic cycle during the simulation to ensure the accuracy of the results. Nine wells are evenly placed in the aquifer to collect the aquifer responses. The computation is implemented in a numeric variable saturated flow model VSAFT2 (Yeh et al., 1993).

2.2. Groundwater Flow Model

VSAFT2 assumes that the 2-D depth-averaged groundwater flow in heterogeneous confined aquifers can be described by

$$\nabla \cdot [T \cdot \nabla h] = S \frac{\partial h}{\partial t} \tag{1}$$

where h represents pressure head (m), T is hydraulic transmissivity (m^2/hr), S is storage coefficient (−), and t represents time (hr).

In this study, we assume that S is spatially uniform and known such that we focus on the estimation of D (m^2/hr; i.e., the ratio of T over S) only and reduce the complexity of the problem. This complexity arises from the fact that in order to identify T and S uniquely, the conditions that (a) the flux or a T value along each streamline and (b) at least at a time interval, at which the hydraulic head undergoes changes, measured everywhere in the entire aquifer must be known (Mao et al., 2013; Yeh et al., 2015). In addition, it is difficult to estimate the S distribution accurately since the area of high cross-correlation between h and S covers only a narrow zone between the observation well and the source of excitation over a short period of time (Sun et al., 2013).

All the results of this experiments (e.g., the groundwater level responses, Figure 2, cross-correlation results, Figures 3–7, and Monte Carlo simulation, Figures 8–11), are expressed in terms of dimensionless variables such that they are scalable. Specifically, the dimensionless distance is defined as
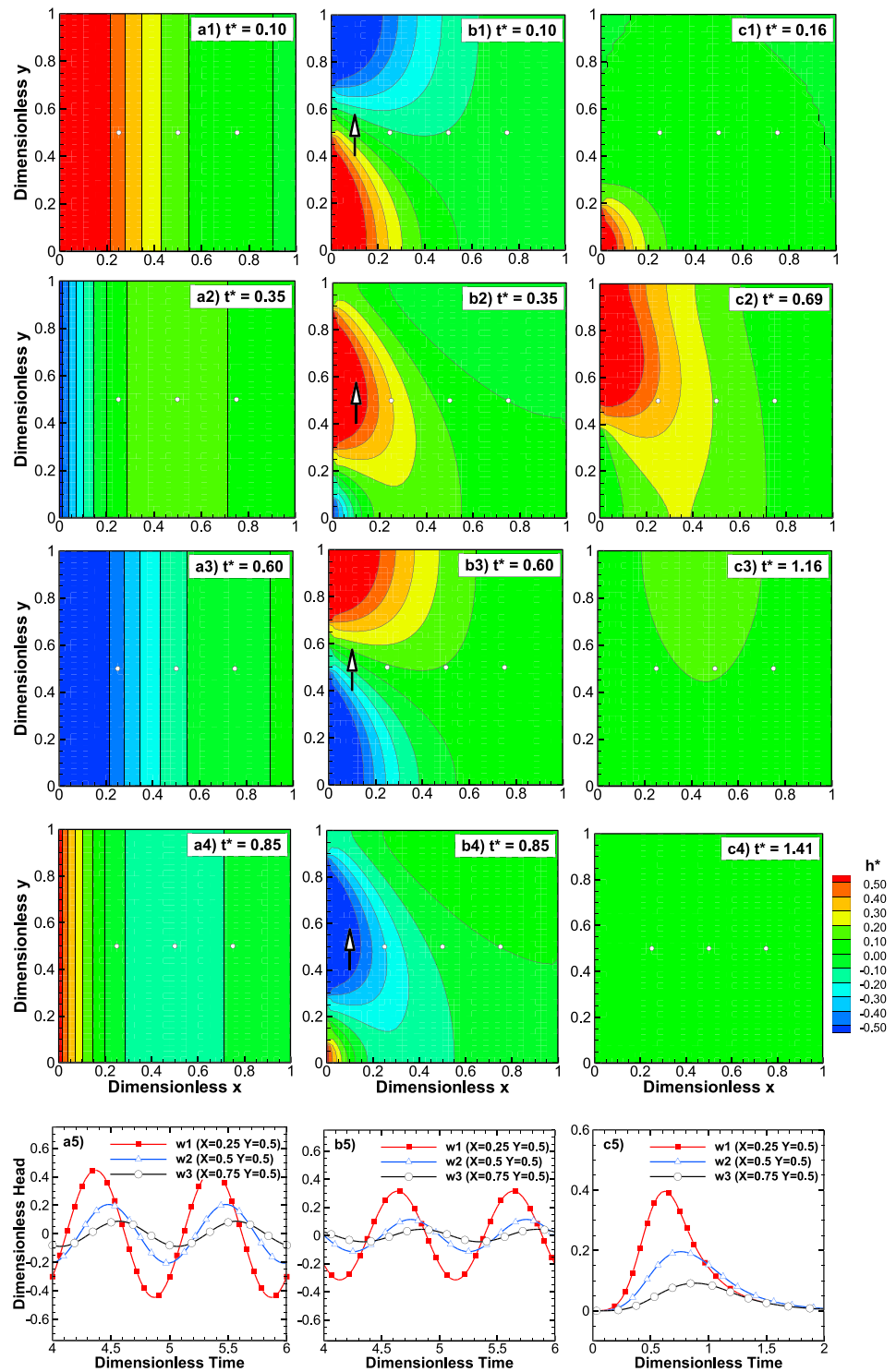
Figure 2. The groundwater level in responses to the (a) static periodic, (b) migrating periodic, and (c) moving single excitations at four different dimensionless time t^* = 0.10, 0.35, 0.60, and 0.85. Figures 2a5–2c5 are the hydrographs corresponding to three observation wells (white circles) at different distances away from the river. The white arrows in Figures 2b1 to 2b4 represent the river flow direction from the upstream to downstream.
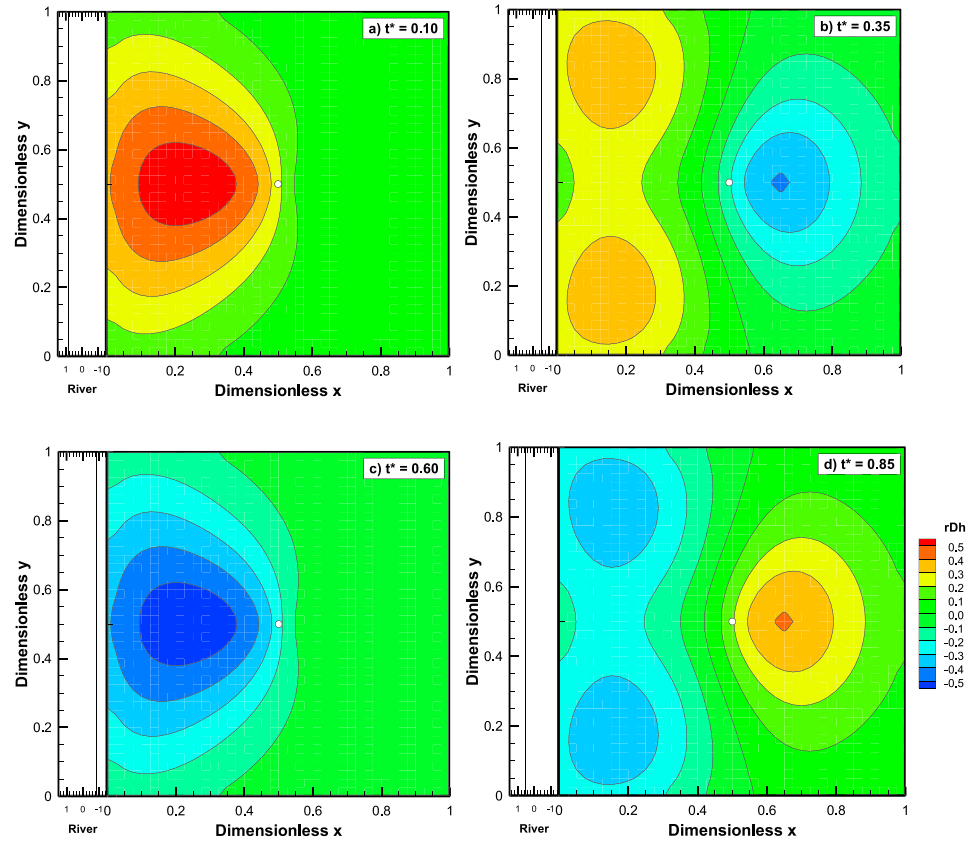
Figure 3. Cross-correlation maps of head with respect to the diffusivity (r_{Dh}) induced by the static periodic excitation with $SNR = 57$ at dimensionless time (a) $t^* = 0.10$, (b) $t^* = 0.35$, (c) $t^* = 0.60$, and (d) $t^* = 0.85$. The white circle is the observation well.

$$x^* = \frac{x}{L_x}, y^* = \frac{y}{L_y} \tag{2}$$

where x and y are the distance from the origin (m). L_x and L_y are the widths of the domain (m) in x and y directions respectively.

The dimensionless time (i.e., phase) is defined as the product of time and frequency ω (cycle/hr)

$$t^* = \omega t \tag{3}$$

The dimensionless water level fluctuation is defined by

$$h^* = \frac{h - h_i}{h_0} \tag{4}$$

where h_0 is the amplitude of the excitation (m) and h_i is the initial head (m). The dimensionless diffusivities in x and y directions are defined by

$$D_x^* = \frac{D}{\omega L_x^2} \ and D_y^* = \frac{D}{\omega L_y^2} \tag{5}$$

The dimensionless correlation lengths are defined as

$$\lambda_x^* = \frac{\lambda_x}{L_x}, \lambda_y^* = \frac{\lambda_y}{L_y} \tag{6}$$

in which λ_x and λ_y are the correlation lengths (m) in x and y directions.
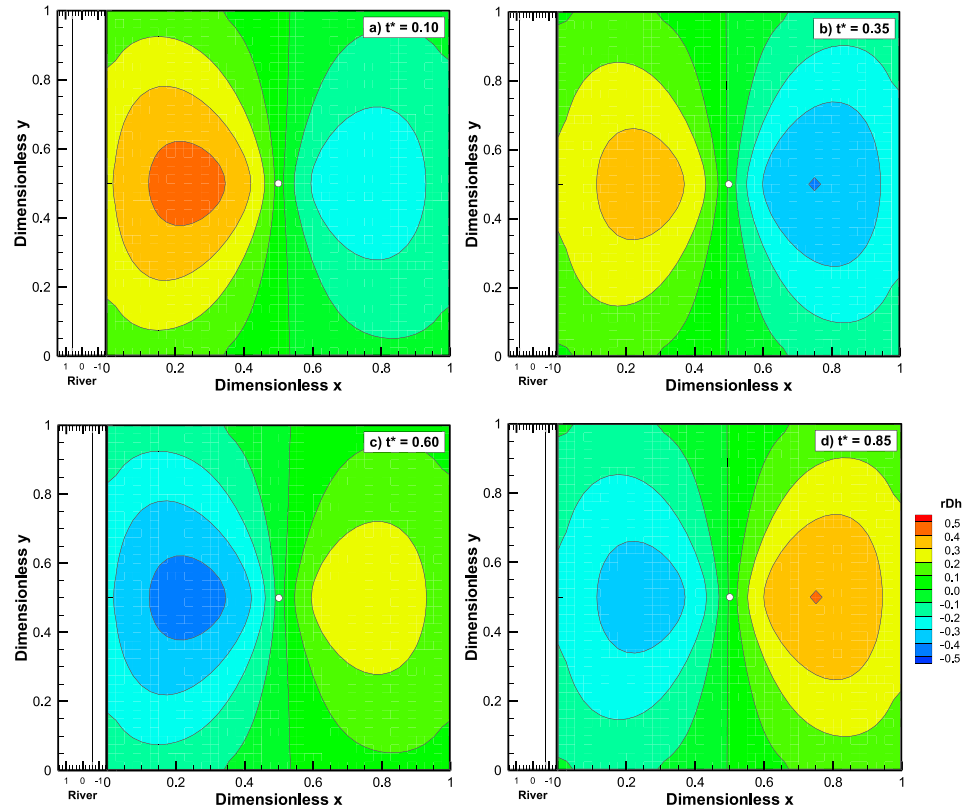
Figure 4. Cross-correlation maps of head with respect to the diffusivity (r_{Dh}) induced by the static periodic excitation with $SNR = 55,000$ at dimensionless time (a) $t^* = 0.10$, (b) $t^* = 0.35$, (c) $t^* = 0.60$, and (d) $t^* = 0.85$. The white circle is the observation well.

2.3. River Stage Fluctuation

The three different river stage variations (static periodic waves, migrating periodic waves, and a moving single excitation) examined are simulated using the following mathematical models.

The static periodic variation (Figure 2a) is expressed as

$$h(t) = h_0 \sin(2\pi\omega t) \tag{7}$$

The variables in the equation have been defined previously. This type of periodic wave intends to represent the annual or seasonal river stage variations of a dammed river, a reservoir, or a perennial river in a watershed where precipitation and runoff are discharged uniformly along the river.

The second form (i.e., migrating periodic) of the excitation (Figure 2b) is modeled by

$$h(x,t) = h_0 \sin(2\pi\omega t + a_x) \tag{8}$$

This represents the periodic fluctuation with some phase lags from the upriver ($y^* = 0$) to downstream ($y^* = 1$). a_x is a function of distance which describes the delay (i.e., phase lag) of river stage variation. This type of migrating periodic wave is to imitate the river stage variation in tidal rivers.

The moving single excitation (Figure 2c) is simulated by the diffusion wave

$$\frac{\partial v(x,t)h(x,t)}{\partial x} + \frac{\partial h(x,t)}{\partial t} = 0 \tag{9}$$

$$g\frac{\partial h(x)}{\partial x} - g(S_0 - S_f) = 0 \tag{10}$$

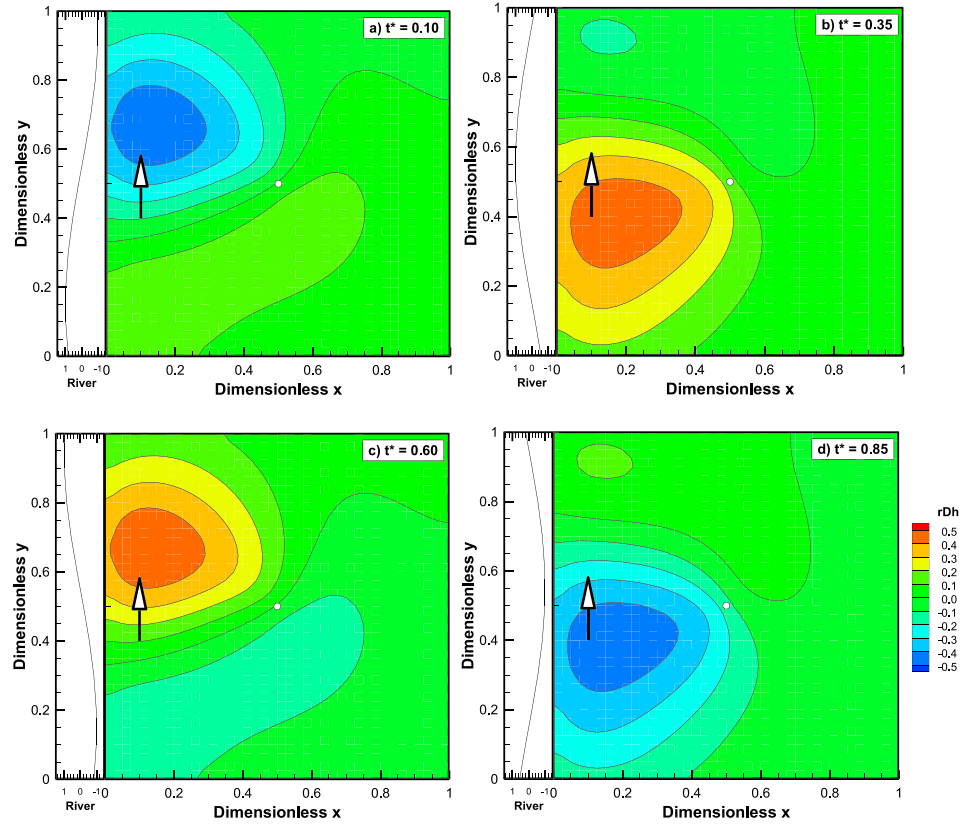with the prescribed boundary conditions

Figure 5. Cross-correlation maps of head with respect to the diffusivity (r_{Dh}) induced by the migrating periodic excitation with $SNR = 57$ at dimensionless time (a) $t^* = 0.10$, (b) $t^* = 0.35$, (c) $t^* = 0.60$, and (d) $t^* = 0.85$. The white circle is the observation well and the white arrow represents the river flow direction from the upstream to downstream.

$$h\left(x, 0 < t \leq 0.5\omega^{-1}\right) = h_0 \sin(2\pi\omega t) \tag{11}$$

$$h\left(x, 0.5\omega^{-1} < t\right) = 0 \tag{12}$$

on the inlet of the river and

$$h(x, t \leq a_t) = 0 \tag{13}$$

$$h\left(x, a_t < t \leq 0.5\omega^{-1} + a_t\right) = h_0 \sin(2\pi\omega t) \tag{14}$$

$$h\left(x, 0.5\omega^{-1} + a_t < t\right) = 0 \tag{15}$$

on the outlet of the river. This moving single excitation is used to depict a short duration perturbation of downstream river stage induced by storm, typhoon, or discharge of reservoir (e.g., hydropeaking). a_t is a function of time describing the delay of river stage propagation from upstream to downstream. g is gravity (m/hr^2). S_0 and S_f are slopes of the river bed and friction (−). v is flow velocity (m/hr).

This paper assumes that the river fully penetrates the confined aquifer and VSAFT2 simulates the pressure propagation, rather than the actual inflow and outflow between the groundwater and the river water. Ideally, a rigorous, fully three-dimensional simulation of the excitations along the river using Navier–Stokes equations or Saint-Venant equations and accounting for the river geometry, riverbed roughness, bank storage, and other factors, as well as a variably saturated flow, describing the interaction of surface and subsurface flow, is more realistic than what we assume here. However, the focus of this study is to examine the effects of different types of excitations on the heterogeneity information carried by the observed heads for the estimation of aquifer properties over large areas. Therefore, the local scale heterogeneities along the riverbed are lumped into the diffusivity values along the river boundary and implicitly included in the flow
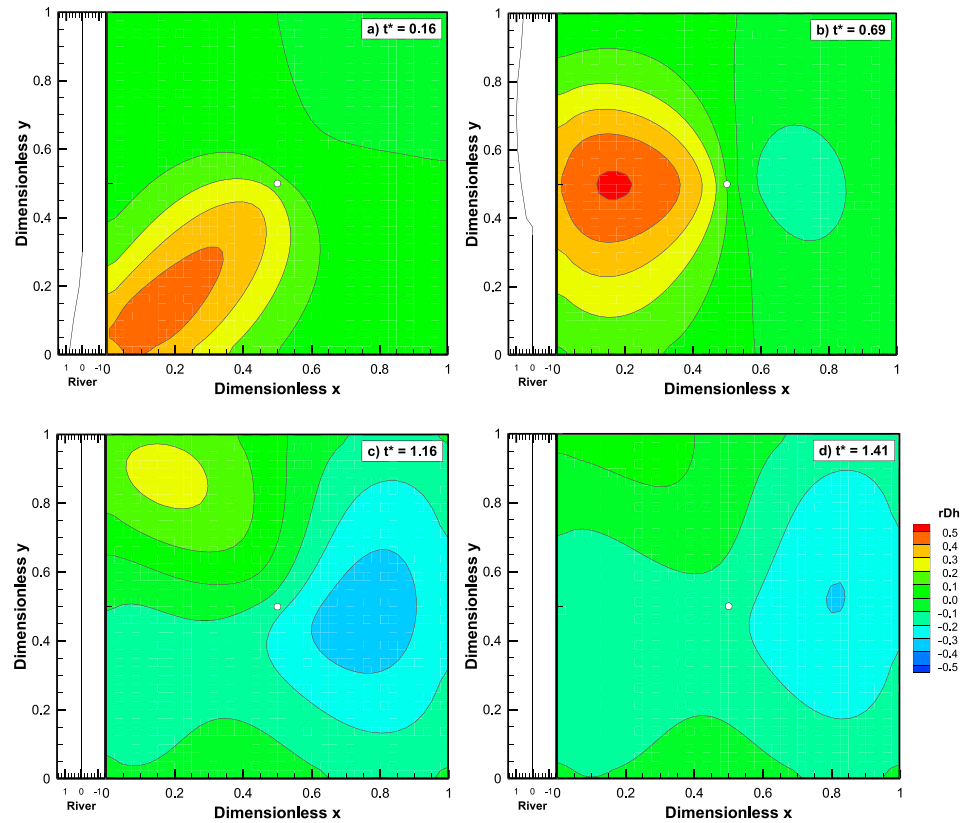
Figure 6. Cross-correlation of head with respect to the diffusivity (r_{Dh}) induced by the moving single excitation with $SNR = 57$ at dimensionless time (a) $t^* = 0.16$, (b) $t^* = 0.69$, (c) $t^* = 1.16$, and (d) $t^* = 1.41$. The white circle is the observation well.

simulation. The omission of the use of detailed simulation approach for river flow would not affect the general conclusion of the study. In effect, this pressure propagation concept is parallel to those used in the analysis of oscillatory pumping (e.g., Black & Kipp, 1981; Cardiff, Barrash, & Kitanidis, 2013 and Rasmussen et al., 2003) for characterizing aquifer.

2.4. Signal-to-Noise Ratio

Factors, such as excitations with different frequencies ω and amplitudes h_0, magnitudes of diffusivity of aquifers D, and distances to the excitation location x, can affect the aquifer responses at observation wells and impact the aquifer characterization efforts. For example, signals of high frequency could decay rapidly with distance such that observed signals at large distance are contaminated by the noise and the calculated heads lose their precisions. As a result, the inverse result may not be reliable. For this reason, the signal-to-noise ratio (SNR) issue is discussed below.

To explain the ratio, we use the analytical solution of the quasi-steady state groundwater head fluctuation in a 1-D semi-infinite homogeneous confined aquifer in response to a periodic head excitation on the boundary. The solution can be expressed as

$$h(x,t) = h_0 \exp\left(-x\sqrt{\frac{\pi\omega}{D}}\right) \sin\left(2\pi\omega t - x\sqrt{\frac{\pi\omega}{D}}\right) \tag{16}$$

in which x (m) is the distance from the excitation (e.g., Carr, 1971). According to the solution, the head attenuation is described by the exponential term while the phase lag is described by the second term in the argument of the sine function. Accordingly, we define the SNR as
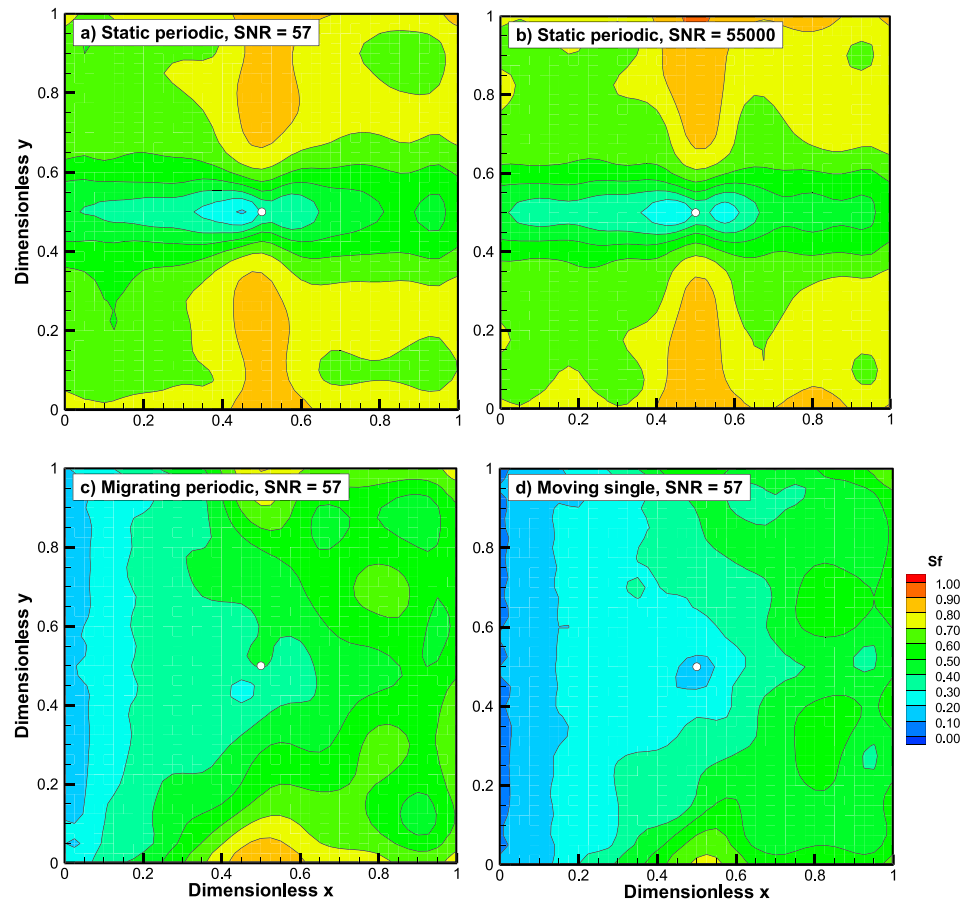
Figure 7. Normalized residual variance of the natural logarithm diffusivity (S_f) after the first iteration with (a) the static periodic excitation with $SNR = 57$, (b) the static periodic excitation with $SNR = 55,000$, (c) the migrating periodic excitation with $SNR = 57$, and (d) the moving single excitation with $SNR = 57$. SNR = signal-to-noise ratio.
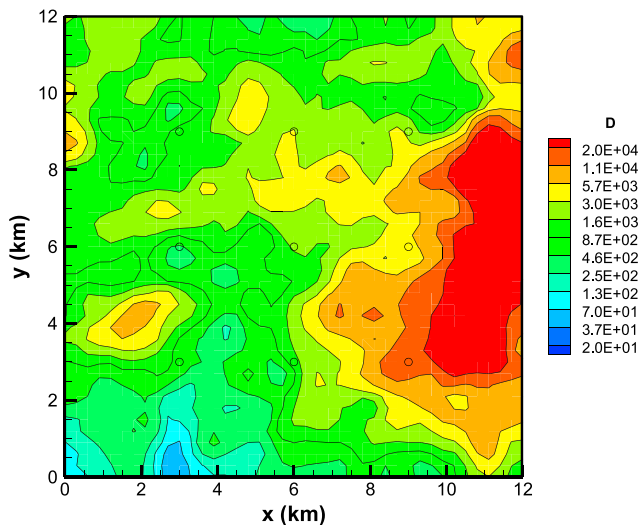

Figure 8. The reference diffusivity D (m^2/hr) field of one realization out of 600. White circles are the observation wells. The variance of ln$D$ equals to 2 (−) and the correlation lengths are 6 (km) along both x and y directions.

$$SNR = \frac{h_0}{h_{err}} \exp\left(-x\sqrt{\frac{\pi\omega}{D}}\right) \tag{17}$$

While the denominator, h_{err}, can be the numerical errors, measurement noise, or model error, in this study, it represents the numerical precision error. The numerical precision of 8 bytes floating point value is about 15 digits, the truncation error of our study is 10^{-7} m, and the round-off error is 10^{-6} m. Thus, we choose $h_{err} = 10^{-5}$ m. While the measurement noise or model errors are usually larger than the numerical error, this choice should not affect the conclusion of this study because our results are expressed in terms of the SNR. That is, the same SNR could be any combined result of the noise level and the magnitude of the aquifer responses, which also depend on the frequency ω, diffusivity D, distance x, and amplitude h_0.

In the cases, where more than one observation wells are used, the arithmetic average of the distances between wells and the excitation is used for x in equation (17). As a result, the head attenuation and the corresponding SNR represent the average of those of the individual well. With this SNR criterion, the observed or simulated head is considered usable if $SNR > 1$, and the estimated Ds are considered accurate
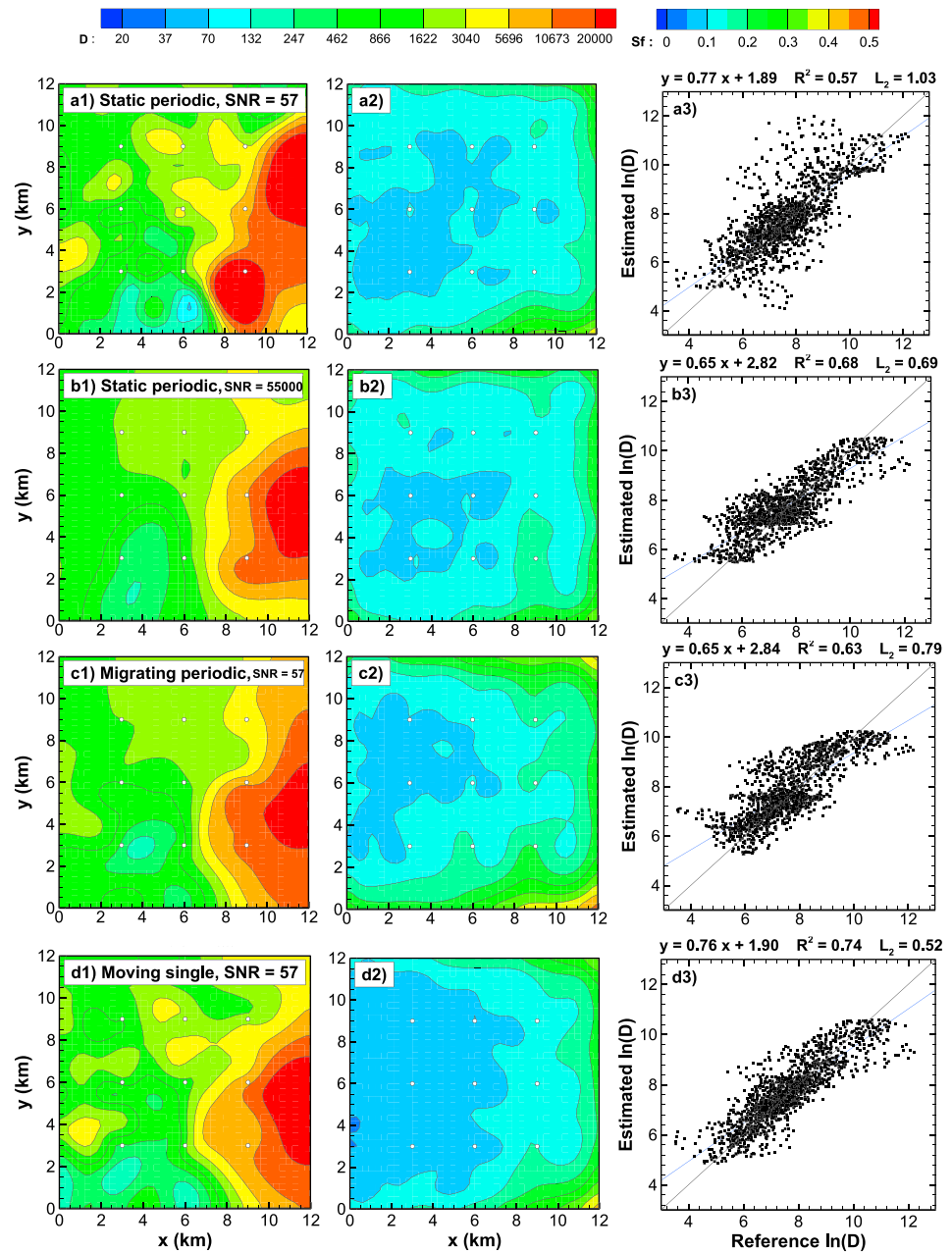
Figure 9. The estimated diffusivity D (m^2/hr), the normalized residual variance of ln$D$ ($-$), and the scatterplots between the reference and estimated values using (a) the static periodic excitation with $SNR = 57$, (b) with $SNR = 55,000$, (c) the migrating periodic excitation with $SNR = 57$, and (d) the moving single excitation with $SNR = 57$. The white circles are the observation wells. SNR = signal-to-noise ratio.

regardless of the values of h_0, x, ω, D, and h_{err}. Notice that for a fixed h_0, x, and D values, a large SNR value implies the frequency of the excitation ω is low and vice versa.

3. Cross-Correlation Analysis

To investigate the effects of different forms of river stage excitations on the estimates of Ds, the successive linear estimator (SLE, section 4; Yeh et al., 1996) is employed. The cross correlation between the observed heads at different times and Ds at different locations of the aquifer (r_{Dh}) is the basis of the SLE (equations (22) and (23)). As a statistical measure of the contribution of the D from various locations to an observed head in
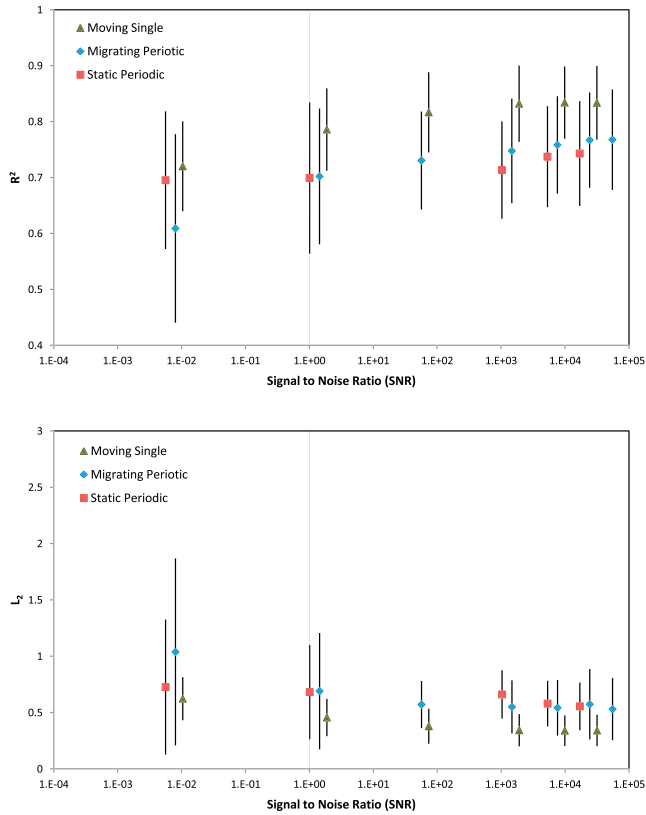
Figure 10. Mean determination coefficient R^2 and mean squared error L_2 between the estimated and reference fields from the static periodic excitation (red square), migrating periodic excitation (blue diamond), and moving single excitation (green triangle) versus SNRs. The solid lines above and below the symbols represent one standard deviation of R^2 and L_2. The dashed line indicates $SNR = 1$. For the clarity of standard deviation, the positions of the static periodic and moving single excitations of each SNR value are slightly shifted in front of and after the symbol of migrating periodic excitation.

an aquifer under a given excitation, r_{Dh} reveals the most likely location, where the D variation contributes the most to the observed head variation. For these reasons, maps of r_{Dh} under static and migrating periodic variations and a moving single excitation along a boundary of an aquifer are discussed below.

The cross-correlation analysis is similar to the sensitivity analysis but it considers the spatial statistics (mean, variance, and correlation length) that depicts heterogeneity is considered (Sun et al., 2013). Suppose during a known excitation event, we have collected a total number of m observed heads in a well at several times from a parameter field consisting of n individual D values. The dimensionless cross correlation $\mathbf{r}_{Dh}(t)$ ($n \times m$) is defined by

$$\mathbf{r}_{Dh}(t) = \frac{\mathbf{J}_{Dh}^T(t)\mathbf{R}_{ff}}{dia\left(\mathbf{R}_{ff}\right)^{0.5}dia\left(\mathbf{J}_{Dh}^T(t)\mathbf{R}_{ff}\mathbf{J}_{Dh}(t)\right)^{0.5}} \quad (18)$$

in which $\mathbf{J}_{Dh}(t)$ ($n \times m$) is the sensitivity of the head at the observation location with respect to hydraulic diffusivity at a given time, t, at everywhere in the domain. $\mathbf{R}_{ff}(n \times n)$ is the unconditional covariance function, depicting the spatial correlation between parameters. The term $dia(\cdot)$ represents the diagonal term of the matrix. In this study, the sensitivity is calculated using an adjoint state approach (e.g., Sun & Yeh, 1990; Sykes et al., 1985), although a simple perturbation approach would work as well. The unconditional covariance function used is given as

$$\mathbf{R}_{ff} = Var \cdot \exp\left(-\sqrt{\frac{\mathbf{d_x}\mathbf{d_x}^T}{\lambda_x^2} + \frac{\mathbf{d_y}\mathbf{d_y}^T}{\lambda_y^2}}\right) \quad (19)$$

in which Var represents the unconditional spatial variance of the parameter D. $\mathbf{d_x}$ ($n \times 1$) and $\mathbf{d_y}$ ($n \times 1$) are the distance between two parameters in x and y directions.

In the following sections, we first investigate the effects of SNR values on the cross-correlation distributions at different times under a static periodic excitation (section 3.1). We intend to show that different SNR values (specifically, signals of different frequencies) lead to similar cross-correlation pattern and in turn the similar estimates. To accomplish this goal, two SNR values are selected. One is at a typical SNR level ($SNR = 57$) and the other is an extremely large SNR value ($SNR = 55,000$) representing the upper bound. The $SNR = 57$ is corresponding to the following river and aquifer characteristics: mean distance to the river x is 5 (km), T is 20 (m^2/day), S is 10^{-6} ($-$), noise level h_{err} is 10^{-3} (m), the river stage variation h_0 is 1.0 (m), period of river ω is 1.0 (day/cycle), and the corresponding groundwater level fluctuation is 5.7 (cm). The $SNR = 55,000$ is corresponding to x is 5 (km), T is 20 (m^2/day), S is 10^{-6} ($-$), h_{err} is 10^{-4} (m), h_0 is 6.5 (m), ω is 365 (day/cycle), and the corresponding groundwater level fluctuation is 5.5 (m). Afterward, we show the cross-correlation distributions at different times under a migrating periodic excitation and a moving single excitation with a given $SNR = 57$ value (sections 3.2 and 3.3). These results are to illustrate the effects of different forms of excitations on the cross-correlation distributions and to emphasize the importance of a tomography survey (a moving excitation source) concept. For all these analyses, the monitoring well is located in the center of the aquifer with a squared label (Figure 1). The dimensionless mean diffusivities D_x^* and D_y^* are 4.67×10^{-4} ($-$) when $SNR = 57$ and are 9.3×10^{-3} when $SNR = 55,000$. The dimensionless correlation lengths λ_x^* and λ_y^* are 0.125 ($-$).

3.1. Static Periodic River Stage Fluctuations

The cross-correlation map, r_{Dh}, corresponding to $SNR = 57$ (i.e., excitation with small amplitude or high frequency since x and D are fixed) at different times are depicted in Figures 3a–3d. The associated river stages
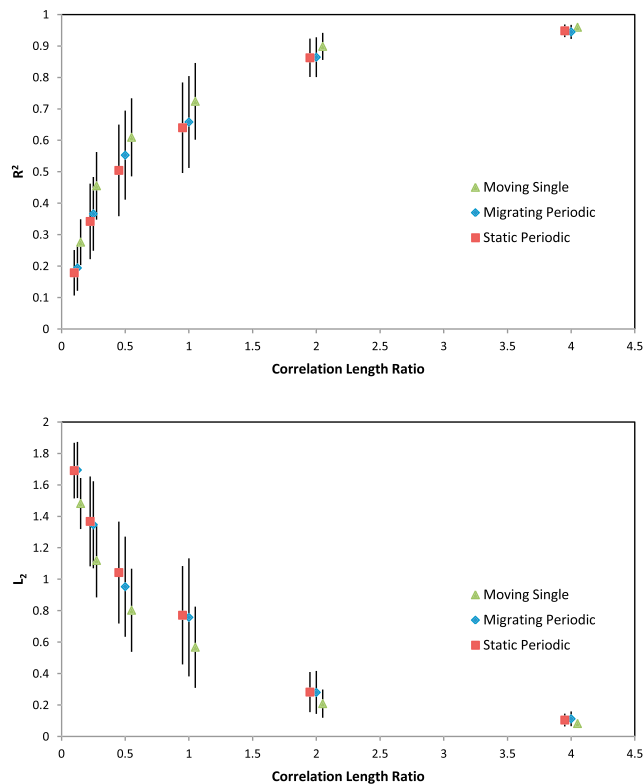
Figure 11. Mean determination coefficient R^2 and mean squared error L_2 between the estimated and reference fields from the static periodic excitation (red square), migrating periodic excitation (blue diamond), and moving single excitation (green triangle) as a function of the ratio of correlation scale to well interval. The solid lines above and below the symbols represent one standard deviation of R^2 and L_2. For the clarity of standard deviation, the positions of the static periodic and moving single excitations of each ratio are slightly shifted in front of and after the symbol of migrating periodic excitation.

are shown on the left panel of each figure. According to Figure 3a, at $t^* = 0.10$, the r_{Dh} forms a mound of positive values between the observation well and the rive boundary. This result indicates that the observed head at the well is likely influenced by the heterogeneity of D at the peak of the mound.

As the river stage approaches its trough ($t^* = 0.35$; Figure 3b), the positive mound splits into two (a saddle shape) parallel to the river: one moving toward the upstream and the other to the downstream. Moreover, a negative mound forms in the area between the well and the right-hand side constant head boundary, with the maximum negative value near the center of this area. This map suggests that the head at the well likely carry information about the heterogeneity at these three mounds.

After the river stage starts to recover from the trough ($t^* = 0.60$; Figure 3c), the r_{Dh} pattern is identical to that in Figure 3a but the value of correlation reverses, attributed to the periodic behavior of the excitations. Likewise, Figure 3d is a mirror image of Figure 3b. These results suggest that aquifer response to periodic variations after half of the cycle carries redundant information about the aquifer characteristics.

The r_{Dh} maps with $SNR = 55,000$ (i.e., excitation with large amplitude or low frequency) at different time steps are plotted in Figures 4a–4d. During the first half cycle when the river stage is above the mean stage, the observed head is positively correlated with D in the area between the river and well and is negatively correlated with D in the area between the well and right-hand side boundary (Figures 4a and 4b). The spatial distributions of r_{Dh} map reverse when the river stage is lower than the average during the second half cycle (Figures 4c and 4d).

3.2. Migrating Periodic Wave

As indicated in Figure 5a, at the early time, $t^* = 0.10$, where the peak of river stage is at upper stream (i.e., $y^* = 0$) and the trough is at the downstream, the observed head is positively correlated with Ds between the well and river near the upstream and is negatively correlated at downstream. Accompanied by the propagation of river stages, the correlation pattern moves downstream (Figure 5b). The maximum positively correlated region appears at the midstream after the peak of stream stage passing through $y^* = 0.5$. Notice that under this circumstance, Ds at the area between the well and right-hand side boundary are almost uncorrelated with the head.

Once the peak of the river stage variation passes the domain, r_{Dh} patterns in Figures 5c and 5d are identical to those shown in Figure 5a and 5b but with reversed signs. Such similarity suggests that the aquifer responses at the well to a moving periodic variation carry the replicated information about the aquifer characteristics. That is to say, only a half of the head collected over a periodic cycle is useful.

3.3. Moving Single Excitation

The river stages and the r_{Dh} maps at different times under a moving single excitation are illustrated in Figure 6. At the early time when the front of the excitation appears at the upper stream, the observed head is positively correlated with Ds between the well and the rising limb of the excitation (Figure 6a). As the excitation moves downstream, the positive r_{Dh} region moves to the middle and the down streams afterward (Figures 6b and 6c). The cross correlation, r_{Dh}, between the well and right-hand side boundary is close to zero at early times. It then evolves into a negative correlation as the excitation is moving through the river. Once the excitation completely passes the river, the groundwater level starts to recover, the absolute value of r_{Dh} everywhere rebounds to zero (Figure 6d). Finally, the water levels at the well returns to their initial values, which is indicative of no information about Ds is available.

As revealed in these figures, differences between r_{Dh} of different times are significant, suggesting that the observed heads at different times carry information about heterogeneity at different parts of the aquifer. This unique characteristic is absent in those of the static and migrating periodic waves. Thus, the moving single excitation constitutes a hydraulic tomography survey using the variation of the river stage.

3.4. Normalized Residual Variance

To further substantiate the findings of sections 3.1, 3.2, and 3.3, a first-order normalized residual variance, $\mathbf{S}_f$ ($n \times 1$), is used to evaluate the impacts of different forms of excitations on the estimates and is defined as

$$\varepsilon_{ff} = \mathbf{R}_{ff} - \mathbf{R}_{ff} \mathbf{J}_{fh} \left[\mathbf{J}_{fh}^T \mathbf{R}_{ff} \mathbf{J}_{fh} \right]^{-1} \mathbf{J}_{fh}^T \mathbf{R}_{ff} \tag{20}$$

$$\mathbf{S}_f = \frac{dia\left[\varepsilon_{ff}\right]}{dia\left[\mathbf{R}_{ff}\right]} \tag{21}$$

in which ε_{ff} ($n \times n$) is the residual covariance matrix.

This equation simply is the residual variance (equation (23)) at first iteration of simultaneous successive linear estimator (SimSLE) normalized by the spatial variance (*Var* in equation (19), uncertainty due to heterogeneity) and represents the amount of uncertainty of the estimated parameter remained after the inclusion of head measurements at the well. If the value of $\mathbf{S}_f$ at a location is close to zero, the uncertainty of the parameter is small, indicative of the effectiveness of the head information for the parameter estimation, and vice versa. Thus, it is a more direct measure than the cross-correlation analysis. However, it is the result of the linear estimate and is in the ensemble sense. Notice that since $\mathbf{S}_f$ considers the spatial correlation between parameters, it is a better choice than the resolution matrix (e.g., Bohling, 2009; Menke, 1989; Paradis et al., 2015; Vasco et al., 1997) when the parameters are spatially correlated.

The normalized residual variance map corresponding to the two static periodic waves with *SNR* = 57 and *SNR* = 55,000 are presented in Figures 7a and 7b. The similarity of the two $\mathbf{S}_f$ maps further corroborates the finding from the cross-correlation maps that the heads collected under these two SNRs (e.g., different in frequency, ω, and amplitude, h_0) infer similar heterogeneity.

The $\mathbf{S}_f$ map of the migrating periodic wave with *SNR* = 57 (Figure 7c), in comparison with those of static periodic waves, reveals that the distributions of the uncertainty of the estimates are quite different. In particular, the uncertainty in the area between the well and stream are reduced significantly. Such difference implies that the water level variation at the observation well in responses to the migrating periodic wave contains more information about the aquifer heterogeneity than that due to the static periodic wave.

As illustrated in Figure 7d, $\mathbf{S}_f$ map for the moving single excitation has a similar spatial pattern to that of migrating periodic wave (Figure 7c) but the uncertainty level is much smaller. Accordingly, we say that the moving single excitation is a more effective excitation than the others, corroborating the results of the above cross-correlation analysis.

4. Parameter Identification

Aforementioned analyses recommend that a moving single excitation is analogous to a hydraulic tomography survey that conducts a series of sequential pumping test or slug test along the river boundary. The next step is to verify this recommendation using a realization and multiple realizations of synthetic heterogeneous aquifers. For this purpose, a SimSLE (Xiang et al., 2009), an extended version of the SLE (Yeh et al., 1996; Zhu & Yeh, 2005), is employed to estimate Ds with observed heads under different excitations. The algorithm of SimSLE is briefly presented below.

4.1. Successive Linear Estimator

Suppose during a known excitation event, we have collected a total number of m observed heads at several times and locations, denoted by $\mathbf{h}^*$ ($m \times 1$). The estimation of conditional effective parameter fields, consisting of n individual D values, is iteratively determined using the following linear estimator:

$$\widehat{\mathbf{f}}^{(r+1)} = \widehat{\mathbf{f}}^{(r)} + \boldsymbol{\varepsilon}_{ff}^{(r)} \mathbf{J}_{fh}^{(r)} \left[\mathbf{J}_{fh}^{(r)T} \boldsymbol{\varepsilon}_{ff}^{(r)} \mathbf{J}_{fh}^{(r)} \right]^{-1} \left[\mathbf{h}^{*} - \mathbf{h}^{(r)} \right] \tag{22}$$

where $\widehat{\mathbf{f}}^{(r)}$ is an $n \times 1$ vector, representing perturbations of the estimated ln$D$ (i.e., the estimates minus the unconditional mean ln$D$. ln denotes the natural logarithm), and the superscript r is the iteration index. $\mathbf{h}^{(r)}$ ($m \times 1$) is the simulated heads at the observation wells, based on the ln$D$ estimated from the rth iteration. If ln$D$ measurements are not available, $\widehat{\mathbf{f}}^{(0)}$ is zero and $\boldsymbol{\varepsilon}_{ff}^{(0)}$ ($n \times n$) is the unconditional $\widehat{\mathbf{f}}^{(0)}$ covariance from geologic information (i.e., $\mathbf{R}_{ff}$ defined in equation (19)). The sensitivity matrix is evaluated using the adjoint state approach. After the linear estimation, the conditional residual covariance of $\widehat{\mathbf{f}}^{(r+1)}$ is calculated by

$$\boldsymbol{\varepsilon}_{ff}^{(r+1)} = \boldsymbol{\varepsilon}_{ff}^{(r)} - \boldsymbol{\varepsilon}_{ff}^{(r)} \mathbf{J}_{fh}^{(r)} \left[\mathbf{J}_{fh}^{(r)T} \boldsymbol{\varepsilon}_{ff}^{(r)} \mathbf{J}_{fh}^{(r)} \right]^{-1} \mathbf{J}_{fh}^{(r)T} \boldsymbol{\varepsilon}_{ff}^{(r)} \tag{23}$$

and the corresponding normalized residual variance is

$$\mathbf{S}_{f}^{(r)} = \frac{dia\left[\boldsymbol{\varepsilon}_{ff}^{(r+1)} \right]}{dia\left[\boldsymbol{\varepsilon}_{ff}^{(0)} \right]} \tag{24}$$

The diagonal term of the residual covariance matrix (i.e., residual variance) represents the remaining uncertainty of the estimated ln$D$ after the head information is included. A small residual variance indicates the spatial trend of estimated ln$D$ is close to the true, while a large value indicates the estimate is close to the initial guessed mean value (i.e., heterogeneity is not resolved).

The estimated field is considered as the final one when either the mean squared error of simulated and observed heads is smaller than a given tolerance or the increase of the spatial variance of the estimated D becomes steady.

Notice that the geostatistical parameters (e.g., unconditional mean D, correlation length of D, and variance of D) utilized to construct $\widehat{\mathbf{f}}^{(0)}$ and $\boldsymbol{\varepsilon}_{ff}^{(0)}$ are specified in advance. They are adjusted by the observed head automatically during the iteration processes (equations (22) and (23)) in terms of the estimated ln$D$ $\widehat{\mathbf{f}}^{(r)}$ and residual variance, $\boldsymbol{\varepsilon}_{ff}^{(r)}$. Nevertheless, when the observed heads are spatially sparse, good prior information of these parameters could enhance the estimates (Tso et al., 2016; Zha et al., 2017). Detailed discussions could be found in Xiang et al. (2009) and a recent publication by Zha et al. (2018).

4.2. Performance Metrics

For evaluation of the estimates, the coefficient of determination (R^2) is utilized to evaluate the similarity between the reference and estimated ln$D$ fields. R^2 is defined as

$$R^2 = \left[\frac{\frac{1}{n} \sum_{i=1}^{n} \left(D_i - \overline{D} \right) \left(\widehat{D}_i - \overline{\widehat{D}} \right)}{std(D) \, std\left(\widehat{D} \right)} \right]^2 \tag{25}$$

where D and $\widehat{D}$ denote the reference and estimated ln$D$ fields, respectively. $\overline{D}$ and $\overline{\widehat{D}}$ represent the average. $std(\cdot)$ stands for the standard deviation. In addition, the mean squared error (i.e., L_2 norm) is adopted to evaluate the differences between reference and estimated fields.

$$L_2 = \frac{1}{n} \sum_{i=1}^{n} \left(D_i - \widehat{D}_i \right)^2 \tag{26}$$

A linear regression model is also used.

4.3. Effects of SNR

In the following experiments, the layout of the aquifer for parameter identification is the same as that in the cross-correlation analysis. With a given correlation scale and measurement interval ratio, 600 random fields

are generated for each given *SNR* value using a spectral method (Gutjahr, 1989; Robin et al., 1993) to investigate its effects on the estimated *D* fields. The initial and boundary conditions are the same as those utilized in the cross-correlation analysis. Nine monitoring wells are evenly distributed in the aquifer to collect the head responses (Figure 1).

For different *SNR* values, we fix the amplitude h_0 at 1 (m) but change the period ω^{-1} (i.e., 32, 160, and 640 (hr/cycle)) and vary the geometric mean *D* of the random fields (i.e., from 0.0045 to 1.8 (km^2/hr)). As a result, the values of *SNR* range from 10^{-12} to 10^6. All the random fields have the variance of ln*D* equals to 2 (−), and the correlation lengths 6 (km) in both *x* and *y* directions. One realization of the random *D* field with geometric mean $D = 1.8$ (km^2/hr) and the given variance and correlation scales is illustrated in Figure 8. This is the *D* field used as the reference field for illustration of the effects of *SNR* on the estimation in one realization, discussed below.

4.3.1. Results of Single Realization

The estimated *D* fields, normalized residual variance $\mathbf{S}_f$, and *D* scatterplot between the reference and estimated *D* for the case using head responses at the nine wells induced by the static periodic excitations with $SNR = 57$ are illustrated in Figures 9a1, 9a2, and 9a3, respectively, and those with $SNR = 55,000$ are in Figures 9b. Similarly, Figures 9c are plots of those corresponding to the migrating periodic excitation with $SNR = 57$. Those based on the moving single excitation with $SNR = 57$ are depicted in Figures 9d. Results of these excitations with $SNR = 55,000$ are omitted since they are similar to those with $SNR = 57$.

A visual comparison of the estimates, using heads from the static periodic head variations with $SNR = 57$ (Figures 9a1–9a3) and $SNR = 55,000$ (Figures 9b1–9b3), indicates that the two estimated fields capture the general pattern of the reference field. Although they have some differences, it is difficult to tell which one is better, even using the normalized residual variance $\mathbf{S}_f$ and performance metrics (i.e., L_2, R^2, and regression line). As we compare the estimates based on the static (Figures 9a) and migrating periodic waves (Figures 9c), again, the estimated *D* fields are similar although the case with the migrating periodic excitation yields slightly deteriorated estimates. On the contrary, dramatic improvement of the estimated and normalized residual variance fields are apparent as head data from the moving single excitation (Figures 9d) is utilized—R^2 improves from around 0.57 to 0.74, while L_2 reduces from about 1.03 to 0.52.

The inconclusive results of the comparisons between $SNR = 57$ and $SNR = 55,000$ and between the static and migrating periodic waves are likely due to the use of a single realization, which may not be representative for all possible realizations. Again, the cross correlation and residual variance presented are based on the ensemble statistics as do the sensitivity and resolution matrix used in other inverse methods. That is, the estimates from any inverse model (geostatistical approach or other approaches) represent the likely *D* field given the observed heads, which will vary from realization to realization unless the problem is well defined or the domain is sufficiently large (i.e., ergodicity issue). Therefore, Monte Carlo simulation is conducted to ensure the conclusiveness of the findings.

4.3.2. Results of Monte Carlo Experiments

Figures 10a and 10b summarize the performances of static periodic, migrating periodic, and moving single excitations in terms of the mean and standard deviation of R^2 and L_2 between the estimated and reference fields.

As displayed in the figures, mean R^2 values are poor when *SNR* values are small and gradually increase with the increase of the *SNR* values. After $SNR > 1$, the mean R^2 values stabilize around 0.70 to 0.78 and L_2 is around 0.55 to 0.69 for either static or migrating periodic excitations. This stabilization of the value suggests no significant differences in the resolutions of estimated fields. The resolution analysis by Paradis et al. (2015) for the tomographic slug test reached the same conclusion. Furthermore, the differences in the mean R^2 values of static and migrating excitation cases are within 0.05—small. In another word, once $SNR > 1$, the differences in the magnitude of aquifer hydraulic properties *D*, the distance between the measurements and excitations *x*, and most importantly, excitation frequency ω and amplitude h_0 have no notable impacts on the resolution of the aquifer characterization. Nevertheless, excitations with low frequencies ω and large amplitudes h_0 enhance the *SNR* value of the observed head at all distances in spite of the aquifer's diffusivity value.

These figures also reveal that the resolution of the estimates using a moving single excitation is better to those from the static or migrating periodic sources. Mean R^2 values range between 0.79 and 0.83 are

better than those of static or migrating periodic excitations. Mean L_2 values between 0.34 and 0.46 are much better as well. The nonredundancy information as implied in the cross-correlation analysis and normalized residual variance (Figures 6 and 7) are the reason. This result is consistent with HT concept (different excitation source locations) and supports the river stage tomography concept demonstrated in the works by Yeh et al. (2008 and 2009) and a recent work by Wang et al. (2017). However, as indicated by the standard deviation, one should be aware that the improvement of using a moving single excitation is not guaranteed for any arbitrary realization. Likewise, the standard deviation also corroborates the ensemble nature of cross-correlation analysis.

4.4. Effects of Correlation Scale and Measurement Interval Ratio

In order to investigate the effects of spatial density of measurement network and the spatial correlation scale of parameter field on the resolution of estimate, the Monte Carlo simulation is used. For this experiment, a spatial sampling index is defined, which is

$$de = \frac{\lambda}{2dw} \tag{27}$$

where dw is the interval between wells (Figure 1). The simulation setups are identical to those for the investigation of the effect of SNR, except the mean D value, correlation length λ, and period ω^{-1}. The spatial geometric mean D value is one (km^2/hr) and the variance of lnD is one ($-$). The period of excitation is fixed at 640 (hr/cycle), leading to a value of 165,000 for SNR. For cases where $de \leq 1$ (i.e., 0.125, 0.25, 0.5, and 1.0), we vary the correlation lengths from 0.75 to 6 (km) while fixed the well interval dw at 3 (km). On the other hand, for cases where $de > 1$ (e.g., 2 and 4), the correlation length is fixed at 6 (km), and dw is reduced to 1.5 and 0.75 (km), that is, the number of well increases to 36 (6×6) and 144 (12×12). For each de value, 600 realizations are used.

The estimate performance statistics (i.e., R^2 and L_2 values of the estimates of the 600 realizations) using the heads in response to the static periodic, migrating periodic, and moving single waves are depicted in Figure 11 as a function of the spatial sampling indexes. As shown in the figure, the mean values of R^2 of all realizations improve from 0.19 to 0.94 and the mean L_2 values decrease from 1.7 to 0.1 as the sampling index increases. The performance deteriorates when $de < 0.5$ (i.e., small correlation length or sparse monitoring network), implying that the signals in response to small-scale heterogeneity are filtered out. The rate of improvement stabilizes at the index around 2. This finding is consistent with the finding by Yeh and Liu (2000) and Cardiff et al. (2013), but we find the sampling interval should be less than a quarter of the correlation scale of the dominant heterogeneity. In addition, the figure shows that the performances of estimate using a moving single wave are better than those with a static or a migrating periodic wave, confirming the finding of the cross-correlation analysis.

4.5. Discussion

As displayed in Figures 10 and 11, the improvements due to the increase of SNR or de values are not guaranteed for each realization as indicated by the standard deviations of R^2 and L_2 of the Monte Carlo results. These nonzero standard deviations are attributed to the ensemble mean nature of the governing flow equation (e.g., equation (1)) and the ergodicity assumption, which is automatically invoked as the equation is applied to a field site (Yeh et al., 2015). Ergodicity means that the spatial statistics equals the ensemble statistics

Specifically, hydraulic properties (e.g., Ds) of an aquifer are inherently heterogeneous. Without knowing the Ds at every location of the aquifer, the governing flow equation simulates the ensemble mean head field (either conditional or unconditional; Yeh et al., 2015, Zha et al., 2017). The ensemble mean head field represents the average of all possible head fields resulting from all possible heterogeneous D fields of the aquifer. As such, the mean head field differs from the true head field. This difference between the mean head field from the true field is then expressed through the ensemble head variance or covariance. Since the mean and variance are ensemble statistics, in order to apply these ensemble statistics to a particular aquifer (one possibility or realization), the D field must be infinitely large so that D and head's spatial statistics of this realization is equivalent to its ensemble statistics. Otherwise, the mean and variance of D, as well as those of heads, would vary from one realization to another as demonstrated in the Monte Carlo

simulation. R^2 and L_2, the ensemble statistics approximated by the spatial statistics (equations (25) and (26)), vary accordingly.

In an infinite domain, the observed head samples all possible heterogeneity due to the diffusive nature of the governing flow equation. In turn, the conditional effective D field, resulting from inverse modeling with observed heads, approaches the ensemble conditional effective D field. The spatial statistics, R^2 and L_2, between the true D fields and the conditional effective D fields are invariant between realizations as a result. For this reason, R^2 and L_2 of results for different realizations are the same and their standard deviations become zero. In other words, ergodicity is met and the spatial statistics equals the ensemble statistics.

On the other hand, if the domain is finite, the mean and variance of simulated heads vary from one realization to another, so does the spatial statistics, R^2 and L_2. Because of this reason, the mean R^2 and L_2 of a larger number of realizations of Monte Carlo simulation are most appropriate for assessing the effectiveness of SNR and de factors on the estimation of D fields as we have done in this study. However, the standard deviations of R^2 and L_2 may remain nonzero.

The nonzero standard deviation again is ascribed to the ergodicity assumption when the ensemble mean equation is applied to a finite domain. For example, in the cases, where SNR effects are investigated, the standard deviations of R^2 and L_2 decrease, as SNR increases but do not approach zero. The decrease reflects the fact that the excitations of low frequencies allow the head to sample heterogeneity over a greater extent of the finite domain than the excitations with high frequencies. The conditional effective D field thus becomes closer to the true one of the finite domains. It, however, is not representative of the entire ensemble (ergodicity assumption is not met) unless the domain is infinite or the inverse problem is well defined as discussed next. As a result, the standard deviation never vanishes.

In the cases where the effects of the correlation scale and sample interval are examined, we observe from Figure 11 that as $de > 2$ (i.e., small sampling intervals), the standard deviations of R^2 and L_2 decrease. They approach zero when de is sufficiently large and the necessary condition for a well-defined inverse problem is closely met. That says, as dense head data are used, the conditional effective D field approaches the true field in each realization and in turn, the standard deviations of R^2 and L_2 become zero. Similarly, when de approaches zero, the mean R^2 approaches zero and the mean L_2 moves toward the variance of the D field. The standard deviations of R^2 and L_2 decrease to zero, accordingly. Again, ergodicity is met and the spatial statistics equals the ensemble statistics. This result holds in spite of the domain size. The above finding (i.e., without considering the ergodicity issue) clearly underscores the inconclusiveness of many works based on one single realization with a finite domain.

The concept of the river stage tomography is valid and is applicable to large-scale groundwater basin as long as the SNR is large. The SNR depends on many factors but mainly the amplitude and frequency of the river stage variation and hydraulic properties of the aquifer as demonstrated in this paper. Separating the river stage signals from signals due to other events (e.g., precipitation, artificial pumping, and many others) could be a challenge. Known characteristics of different natural or anthropogenic events could be helpful for this purpose since the groundwater responses likely carry characteristics of these events, which may be different from the river stage variation. Wavelet (Wang et al., 2017) and independent component analysis (Hsiao et al., 2017) are potential tools to cope with the impacts of other excitations.

Notice that the analysis presented in this paper used depth-averaged groundwater flow model. As such, the simulated groundwater responses represent depth-averaged behaviors of the aquifer and estimated hydraulic heterogeneity is limited in the horizontal plane. Of course, employing a three-dimensional model that considers flow through variably saturated geologic media for this analysis would be more ideal and would allow mapping three-dimensional distribution of heterogeneity including the unsaturated hydraulic properties as reported in HT study by Mao et al. (2013). However, the area where the unsaturated hydraulic properties can be identified is likely restricted in the vicinity of the river. Furthermore, knowledge of fluxes at the river bed would make the inherently ill-defined problem better defined since it is one of the necessary conditions for a well-defined inverse problem (Mao, Yeh, Wan, Hsu, et al., 2013; Yeh et al., 2015 and 2015). Effects of using the prescribed head boundary (river stages) on the unknown flux boundary conditions are limited to the area near the boundary [Figure 4 in Sun et al., 2013]

5. Conclusion

Our analysis confirms that the periodic river stage variations (e.g., seasonal or annual) are viable excitation sources for river stage tomography to delineate large-scale subsurface heterogeneity. The moving single excitation (such as a flash flood event), however, is more effective than the periodic excitations. It can yield more information about aquifer heterogeneity than the others. As such, it is suitable for characterizing not only the large-scale D heterogeneity but also detailed D variations. This finding is consistent with the HT concept and supports the river stage tomography.

Monte Carlo experiment substantiates the ensemble nature of cross-correlation analysis (as well as sensitivity analysis) and residual variance concept. Nevertheless, in the ensemble sense, the Monte Carlo results reveal that once the magnitude of the head response is greater than that of the noise (i.e., $SNR > 1$), the performance metrics (R^2 and L_2) of aquifer characterization based on static or migrating periodic excitations are similar. In other words, with the same number of observation wells (i.e., monitoring network) at a given field site, influences of the differences in the magnitude and frequency of the excitation on mapping the heterogeneity is likely insignificant and inconclusive, although the excitations with low frequencies and large amplitudes enhance the SNR value of the observed head at all distances.

The result of this study further recommends that an effective monitoring network should place wells at an interval less than or equal to a quarter of the correlation length of the dominant aquifer heterogeneity of our interest. That is to say, one cannot expect to better resolve the geological heterogeneity of correlation lengths smaller than this well interval.

Lastly, more synthetic case studies in various hydrogeological contexts and field experiments are needed to fully assess the power of the river stage tomography and the results of this study.

References

Barlow, P. M., Desimone, L. A., & Moench, A. F. (2000). Aquifer response to stream-stage and recharge variations, II, Convolution method and applications. *Journal of Hydrology*, *230*(3-4), 211–229. https://doi.org/10.1016/S0022-1694(00)00176-1

Berg, S. J., & Illman, W. A. (2011). Three-dimensional transient hydraulic tomography in a highly heterogeneous glaciofluvial aquifer-aquitard system. *Water Resources Research*, *47*, W10507. https://doi.org/10.1029/2011WR010616

Berg, S. J., & Illman, W. A. (2013). Field study of subsurface heterogeneity with steady-state hydraulic tomography. *Groundwater*, *51*(1), 29–40. https://doi.org/10.1111/j.1745-6584.2012.00914.x

Black, J. H., & Kipp, K. L. Jr. (1981). Determination of hydrogeological parameters using sinusoidal pressure tests: A theoretical appraisal. *Water Resources Research*, *17*(3), 686–692. https://doi.org/10.1029/WR017i003p00686

Bohling, G. C. (2009). Sensitivity and resolution of tomographic pumping in an alluvial aquifer. *Water Resources Research*, *45*, W02420. https://doi.org/10.1029/2008WR007249

Bohling, G. C., Zhan, X., Butler, J. J. Jr., & Zheng, L. (2002). Steady shape analysis of tomographic pumping tests for characterization of aquifer heterogeneities. *Water Resources Research*, *38*(12), 60-1. https://doi.org/10.1029/2001WR001176

Brauchler, R., Cheng, J., Everette, M., Johnson, B., Dietrich, P., Liedl, R., & Sauter, M. (2007). An inversion strategy for hydraulic tomography: coupling travel time and amplitude inversion. *Journal of Hydrology*, *345*(3-4), 184–198. https://doi.org/10.1016/j.jhydrol.2007.08.011

Brauchler, R., Hu, R., Dietrich, P., & Sauter, M. (2011). A field assessment of high-resolution aquifer characterization based on hydraulic travel time and hydraulic attenuation tomography. *Water Resources Research*, *47*, W03503. https://doi.org/10.1029/2010WR009635

Brauchler, R., Hu, R., Hu, L., Jimenez, S., Bayer, P., Dietrich, P., & Ptak, T. (2013). Rapid field application of hydraulic tomography for resolving aquifer heterogeneity in unconsolidated sediments. *Water Resources Research*, *49*, 2013–2024. https://doi.org/10.1002/wrcr.20181

Brauchler, R., Liedl, R., & Dietrich, P. (2003). A travel time based hydraulic tomographic approach. *Water Resources Research*, *39*(12), 1370. https://doi.org/10.1029/2003WR002262

Brunner, P., Therrien, R., Renard, P., Simmons, C. T., & Franssen, H.-J. H. (2017). Advances in understanding river-groundwater interactions. *Reviews of Geophysics*, *55*, 818–854. https://doi.org/10.1002/2017RG000556

Cardiff, M., Bakhos, T., Kitanidis, P. T., & Barrash, W. (2013). Aquifer heterogeneity characterization with oscillatory pumping: Sensitivity analysis and imaging potential. *Water Resources Research*, *49*, 5395–5410. https://doi.org/10.1002/wrcr.20356

Cardiff, M., Barrash, W., & Kitanidis, P. K. (2012). A field proof-of-concept of aquifer imaging using 3-D transient hydraulic tomography with modular, temporarily-emplaced equipment. *Water Resources Research*, *48*, W05531. https://doi.org/10.1029/2011WR011704

Cardiff, M., Barrash, W., & Kitanidis, P. K. (2013). Hydraulic conductivity imaging from 3-D transient hydraulic tomography at several pumping/observation densities. *Water Resources Research*, *49*, 7311–7326. https://doi.org/10.1002/wrcr.20519

Carr, P. A. (1971). Use of harmonic analysis to study tidal fluctuations in aquifers near the sea. *Water Resources Research*, *7*(3), 632–643. https://doi.org/10.1029/WR007i003p00632

Duffy, C. J., Gelhar, L. W., & Gross, G. W. (1978). Recharge and groundwater conditions in the western region of the Roswell Basin. Report no. 100, New Mexico Water Resources Research Institute, New Mexico State University, Las Cruces, New Mexico, USA.

Ferris, J. G. (1952). Cyclic fluctuations of water level as a basis for determining aquifer transmissibility. U.S. Geological Survey, Ground-Water Hydraulics Section, Contribution No. 1, 17 p. https://doi.org/10.3133/70133368

Ferris, J. G., Knowles, D. B., Brown, R. H., & Stallman, R. W. (1963). Theory of aquifer tests, U.S. Geological Survey Water-Supply Paper 1536 E,174 p. https://doi.org/10.3133/wsp1536E

Gelhar, L. W. (1974). Stochastic analysis of phreatic aquifers. *Water Resources Research*, *10*(3), 539–545. https://doi.org/10.1029/WR010i003p00539

Gelhar, L. W., Gross, G. W., & Duffy, C. J. (1979). Stochastic methods of analysing groundwater recharge. In: The Hydrology of Areas of Low Precipitation (Proceeding of the Canberra Symposium), IAHS Publ. no. 128, 313-321.

Gutjahr, A. L. (1989). Fast Fourier transforms for random field generation, project report for Los Alamos grant, Contract 4-R58-2690R, Dep. of Math., N. M. Tech., Socorro.

Hochstetler, D. L., Barrash, W., Leven, C., Cardiff, M., Chidichimo, F., & Kitanidis, P. K. (2016). Hydraulic tomography: Continuity and discontinuity of high-K and low-K zones. *Groundwater*, *54*(2), 171–185. https://doi.org/10.1111/gwat.12344

Hsiao, C.-T., Chang, L.-C., Tsai, J.-P., & Chen, Y.-C. (2017). Features of spatiotemporal groundwater head variation using independent component analysis. *Journal of Hydrology*, *547*, 623–637. https://doi.org/10.1016/j.jhydrol.2017.02.021

Huang, S.-Y., Wen, J.-C., Yeh, T.-C. J., Lu, W., Juan, H.-L., Tseng, C.-M., et al. (2011). Robustness of joint interpretation of sequential pumping tests: Numerical and field experiments. *Water Resources Research*, *47*, W10530. https://doi.org/10.1029/2011WR010698

Jardani, A., Dupont, J. P., Revil, A., Massei, N., Fournier, M., & Laignel, B. (2012). Geostatistical inverse modeling of the transmissivity field of a heterogeneous alluvial aquifer under tidal influence. *Journal of Hydrology*, *472-473*, 287–300. https://doi.org/10.1016/j.jhydrol.2012.09.031

Jiao, J. J., & Tang, Z. (1999). An analytical solution of groundwater response to tidal fluctuation in a leaky confined aquifer. *Water Resources Research*, *35*(3), 747–751. https://doi.org/10.1029/1998WR900075

Li, H., & Jiao, J. J. (2001). Analytical studies of groundwater-head fluctuation in a coastal confined aquifer overlain by a semi-permeable layer with storage. *Advances in Water Resources*, *24*(5), 565–573. https://doi.org/10.1016/S0309-1708(00)00074-9

Li, H., Jiao, J. J., Luk, M., & Cheung, H. (2002). Tide-induced groundwater level fluctuation in coastal aquifers bounded by L-shaped coastlines. *Water Resources Research*, *38*(3), 6-1. https://doi.org/10.1029/2001WR000556

Li, L., Barry, D. A., Cunningham, C., Stagnitti, F., & Parlange, J. Y. (2000). A two-dimensional analytical solution of groundwater responses to tidal loading in an estuary and ocean. *Advances in Water Resources*, *23*(8), 825–833. https://doi.org/10.1016/S0309-1708(00)00016-6

Li, W., Englert, A., Cirpka, O. A., & Vereecken, H. (2008). Three-dimensional geostatistical inversion of flowmeter and pumping test data. *Groundwater*, *46*(2), 193–201. https://doi.org/10.1111/j.1745-6584.2007.00419.x

Mao, D., Yeh, T.-C. J., Wan, L., Hsu, K.-C., Lee, C.-H., & Wen, J.-C. (2013). Necessary conditions for inverse modeling of flow through variably saturated porous media. *Advances in Water Resources*, *52*, 50–61. https://doi.org/10.1016/j.advwatres.2012.08.001

Mao, D., Yeh, T.-C. J., Wan, L., Lee, C.-H., Hsu, K.-C., Wen, J.-C., & Lu, W. (2013). Cross-correlation analysis and information content of observed heads during pumping in unconfined aquifers. *Water Resources Research*, *49*, 713–731. https://doi.org/10.1002/wrcr.20066

Menke, W. (1989). *Geophysical data analysis: Discrete inverse theory*, rev. ed. (p. 289). United States: Academic Press. https://doi.org/10.1016/B978-0-12-397160-9.00019-9

Moench, A. F., & Barlow, P. M. (2000). Aquifer response to stream-stage and recharge variations: I. Analytical step-response functions. *Journal of Hydrology*, *230*(3-4), 192–210. https://doi.org/10.1016/S0022-1694(00)00175-X

Nevulis, R. H., Davis, D. R., & Sorooshian, S. (1989). Analysis of natural groundwater level variations for hydrogeologic conceptualization, Hanford Site, Washington. *Water Resources Research*, *25*(7), 1519–1529. https://doi.org/10.1029/WR025i007p01519

Paradis, D., Gloaguen, E., Lefebvre, R., & Giroux, B. (2015). Resolution analysis of tomographic slug test head data: Two-dimensional radial case. *Water Resources Research*, *51*, 2356–2376. https://doi.org/10.1002/2013WR014785

Paradis, D., Gloaguen, E., Lefebvre, R., & Giroux, B. (2016). A field proof-of-concept of tomographic slug tests in an anisotropic littoral aquifer. *Journal of Hydrology*, *536*, 61–73. https://doi.org/10.1016/j.jhydrol.2016.02.041

Pinder, G. F., Bredehoeft, J. D., & Cooper, H. H. Jr. (1969). Determination of aquifer diffusivity from aquifer response to fluctuations in river stage. *Water Resources Research*, *5*(4), 850–855. https://doi.org/10.1029/WR005i004p00850

Promma, K., Zheng, C., & Asnachinda, P. (2007). Groundwater and surface-water interactions in a confined alluvial aquifer between two rivers: Effects of groundwater flow dynamics on high iron anomaly. *Hydrogeology Journal*, *15*(3), 495–513. https://doi.org/10.1007/s10040-006-0110-8

Ramirez-Hernandez, J., Hinojosa-Huerta, O., Peregrina-Llanes, M., Calvo-Fonseca, A., & Carrera-Villa, E. (2013). Groundwater responses to controlled water releases in the Limitrophe Region of the Colorado River: implications for management and restoration. *Ecological Engineering*, *59*, 93–103. https://doi.org/10.1016/j.ecoleng.2013.02.016

Rasmussen, T. C., Haborak, K. G., & Young, M. H. (2003). Estimating aquifer hydraulic properties using sinusoidal pumping at the Savannah River Site, South Carolina, USA. *Hydrogeology Journal*, *11*(4), 466–482. https://doi.org/10.1007/s10040-003-0255-7

Robin, M. J. L., Gutjahr, A. L., Sudicky, E. A., & Wilson, J. L. (1993). Cross-correlated random field generation with the direct Fourier transform method. *Water Resources Research*, *29*(7), 2385–2397. https://doi.org/10.1029/93WR00386

Sanchez-León, E., Leven, C., Haslauer, C. P., & Cirpka, O. A. (2016). Combining 3D hydraulic tomography with tracer tests for improved transport characterization. *Groundwater*, *54*(4), 498–507. https://doi.org/10.1111/gwat.12381

Sophocleous, M. A. (1991). Stream-floodwave propagation through the Great Bend alluvial aquifer, Kansas: Field measurements and numerical simulations. *Journal of Hydrology*, *124*(3-4), 207–228. https://doi.org/10.1016/0022-1694(91)90015-A

Straface, S., Fallico, C., Troisi, S., Rizzo, E., & Revil, A. (2007). An inverse procedure to estimate transmissivity from heads and SP signals. *Groundwater*, *45*(4), 420–428. https://doi.org/10.1111/j.1745-6584.2007.00310.x

Sun, H. (1997). A two-dimensional analytical solution of groundwater response to tidal loading in an estuary. *Water Resources Research*, *33*(6), 1429–1435. https://doi.org/10.1029/97WR00482

Sun, N.-Z., & Yeh, W. W.-G. (1990). Coupled inverse problems in groundwater modeling: 1. Sensitivity analysis and parameter identification. *Water Resources Research*, *26*(10), 2507–2525. https://doi.org/10.1029/WR026i010p02507

Sun, R., Yeh, T.-C. J., Mao, D., Jin, M., Lu, W., & Hao, Y. (2013). A temporal sampling strategy for hydraulic tomography analysis. *Water Resources Research*, *49*, 3881–3896. https://doi.org/10.1002/wrcr.20337

Sykes, J. F., Wilson, J. L., & Andrews, R. W. (1985). Sensitivity analysis for steady-state groundwater flow using adjoint operators. *Water Resources Research*, *21*(3), 359–371. https://doi.org/10.1029/WR021i003p00359

Tang, Z., & Jiao, J. J. (2001). A two-dimensional analytical solution for groundwater flow in a leaky confined aquifer system near open tidal water. *Hydrological Processes*, *15*(4), 573–585. https://doi.org/10.1002/hyp.166

Tso, C.-H. M., Zha, Y., Yeh, T.-C. J., & Wen, J.-C. (2016). The relative importance of head, flux, and prior information in hydraulic tomography analysis. *Water Resources Research*, *52*, 3–20. https://doi.org/10.1002/2015WR017191

Vasco, D. W., Datta-Gupta, A., & Long, J. C. S. (1997). Resolution and uncertainty in hydrologic characterization. *Water Resources Research*, *33*(3), 379–397. https://doi.org/10.1029/96WR03301

Vazquez-Sune, E., Capino, B., Abarca, E., & Carrera, J. (2007). Estimation of recharge from floods in disconnected stream-aquifer systems. *Groundwater*, *45*(5), 579–589. https://doi.org/10.1111/j.1745-6584.2007.00326.x

Wang, Y.-L., Yeh, T.-C. J., Wen, J.-C., Huang, S.-Y., Zha, Y., Tsai, J.-P., et al. (2017). Characterizing subsurface hydraulic heterogeneity of alluvial fan using riverstage fluctuations. *Journal of Hydrology*, *547*, 650–663. https://doi.org/10.1016/j.jhydrol.2017.02.032

Xiang, J., Yeh, T.-C. J., Lee, C.-H., Hsu, K.-C., & Wen, J.-C. (2009). A simultaneous successive linear estimator and a guide for hydraulic tomography analysis. *Water Resources Research*, *45*, W02432. https://doi.org/10.1029/2008WR007180

Yeh, T.-C. J., Jin, M., & Hanna, S. (1996). An iterative stochastic inverse method: conditional effective transmissivity and hydraulic head fields. *Water Resources Research*, *32*(1), 85–92. https://doi.org/10.1029/95WR02869

Yeh, T.-C. J., Khaleel, R., & Carroll, K. C. (2015). *Flow through heterogeneous geologic media*. Cambridge, England: Cambridge University Press. https://doi.org/10.1017/CBO9781139879323

Yeh, T.-C. J., & Lee, C. (2007). Time to change the way we collect and analyze data for aquifer characterization. *Groundwater*, *45*(2), 116–118. https://doi.org/10.1111/j.1745-6584.2006.00292.x

Yeh, T.-C. J., Lee, C.-H., Hsu, K.-C., Illman, W. A., Barrash, W., Cai, X., et al. (2008). A view toward the future of subsurface characterization: CAT scanning groundwater basins. *Water Resources Research*, *44*, W03301. https://doi.org/10.1029/2007WR006375

Yeh, T.-C. J., & Liu, S. (2000). Hydraulic tomography: Development of a new aquifer test method. *Water Resources Research*, *36*(8), 2095–2105. https://doi.org/10.1029/2000WR900114

Yeh, T.-C. J., Mao, D., Zha, Y., Wen, J.-C., Wan, L., Hsu, K.-C., & Lee, C.-H. (2015). Uniqueness, scale, and resolution issues in groundwater model parameter identification. *Water Science and Engineering*, *8*(3), 175–194. https://doi.org/10.1016/j.wse.2015.08.002

Yeh, T.-C. J., Xiang, J., Suribhatla, R. M., Hsu, K.-C., Lee, C.-H., & Wen, J.-C. (2009). Riverstage tomography: A new approach for characterizing groundwater basins. *Water Resources Research*, *45*, W05409. https://doi.org/10.1029/2008WR007233

Yeh, T. J., Srivastava, R., Guzman, A., & Harter, T. (1993). A numerical model for water flow and chemical transport in variably saturated porous media. *Groundwater*, *31*(4), 634–644. https://doi.org/10.1111/j.1745-6584.1993.tb00597.x

Zha, Y., Yeh, T.-C. J., Illman, W. A., Onoe, H., Mok, C. M. W., Wen, J.-C., et al. (2017). Incorporating geologic information into hydraulic tomography: A general framework based on geostatistical approach. *Water Resources Research*, *53*, 2850–2876. https://doi.org/10.1002/2016WR019185

Zha, Y., Yeh, T.-C. J., Illman, W. A., Zeng, W., Zhang, Y., Sun, F., & Shi, L. (2018). A reduced-order successive linear estimator for geostatistical inversion and its application in hydraulic tomography. *Water Resources Research*, *54*(3), 1616–1632. https://doi.org/10.1002/2017WR021884

Zha, Y., Yeh, T.-C. J., Shi, L., Huang, S.-Y., Wang, W., & Wen, J.-C. (2017). Quasi-steady state conditions in heterogeneous aquifers during pumping tests. *Advances in Water Resources*, *106*, 95–110. https://doi.org/10.1016/j.advwatres.2017.03.017

Zhao, Z., & Illman, W. A. (2017). On the importance of geological data for three-dimensional steady-state hydraulic tomography at a highly heterogeneous aquifer-aquitard system. *Journal of Hydrology*, *544*, 640–657. https://doi.org/10.1016/j.jhydrol.2016.12.004

Zhu, J., & Yeh, T.-C. J. (2005). Characterization of aquifer heterogeneity using transient hydraulic tomography. *Water Resources Research*, *41*, W07028. https://doi.org/10.1029/2004WR003790